

# Computational comparison of Bragg scattering and TDS intensity in a TEM at different temperatures using a gadolinium crystal

10 credit project course report

Paul M. Zeiger

Supervisor: Jan Rusz  
Uppsala Universitet spring semester 2015

September 11, 2015

---

## Abstract

Gadolinium-157 undergoes a magnetic transition from a ferromagnetic state to a strongly paramagnetic state when it is heated above approximately 20 °C. Nearby this temperature a substantial magnetocaloric effect has been observed. One idea to study this process is to use the features of a transmission electron microscope diffraction pattern. This project aims to provide some calculations on the relation between thermal diffuse scattering and Bragg scattering at different temperatures between 5 K and 350 K of the specimen as well as up to which degree of accuracy one might be able to determine the temperature experimentally by measuring this relation. The thermal vibrations are simulated using a Nosé-Hoover thermostat. The scattered electron intensity is calculated using the real space multislice method.

# Contents

|  |           |
|--|-----------|
| <b>1. Introduction</b>   | <b>1</b>  |
| <b>2. Theory</b>   | <b>1</b>  |
| 2.1. Lattice vibrations . . . . .  | 1         |
| 2.2. Transmission electron microscopy . . . . .  | 2         |
| 2.3. Fast electron approximation of the Schrödinger equation . . . . .                             | 4         |
| 2.4. The Real Space Multislice method (RS-MS) . . . . .  | 5         |
| 2.5. Frozen phonon approximation . . . . .   | 7         |
| <b>3. Method</b>   | <b>8</b>  |
| 3.1. Setting up the multislice code . . . . .  | 11        |
| 3.2. Setting up thermal vibration simulation . . . . .   | 12        |
| 3.3. Integrating the TDS and Bragg spot intensity in the final diffraction pattern . . . . .       | 12        |
| <b>4. Computational results</b>  | <b>15</b> |
| 4.1. Mean square displacement of the atoms . . . . .   | 15        |
| 4.2. Comparison of the intensity of the Bragg scattering with thermal diffuse scattering . . . . . | 18        |
| <b>5. Discussion</b>   | <b>18</b> |
| <b>6. Conclusion</b>   | <b>19</b> |
| <b>7. Prospect</b>   | <b>20</b> |
| <b>A. LAMMPS input files</b>   | <b>22</b> |
| A.1. Optimisation of the Lennard-Jones potential . . . . .   | 22        |
| A.2. Thermal vibrations simulation . . . . .   | 28        |

---

## List of Figures

|     |  |    |
|-----|--|----|
| 1.  | Infinite chain of atoms of mass $M$ , spring constant $\gamma$ and lattice parameter $a$ . . . . .   | 1  |
| 2.  | Schematic overview of the components of a TEM and a sketch of the convergence angle.   | 2  |
| 3.  | Comparison of excerpts of a computer simulated diffraction pattern in reciprocal space with different convergence angles $\alpha$ without thermal vibrations. The colors encode the magnitude of the electron's wave function's probability amplitude $\sqrt{ \Psi ^2}$ . . . . .  | 4  |
| 4.  | Schematic drawing of the crystal slices in the multislice approach. . . . .  | 5  |
| 5.  | Real Gadolinium crystal structure with unit cell parameters $a$ , $b$ , $c$ (compare text for the values) and the computed sum of the potential energies $E$ of the atoms in one unit cell for small deviation from the expected minimum volume $V_0$ for the real Gadolinium structure. . . . .   | 9  |
| 6.  | Modified unit cell with unit cell parameters $a_{\text{new}}$ , $b_{\text{new}}$ and $c_{\text{new}}$ (compare text for the values) as well as results of the sum $E$ of the potential energies in the unit cell and the corresponding Birch-Murnaghan fit. $\sigma_{\text{init}} = 2^{-1/6}b$ is kept the same as in figure 5. . . . .  | 10 |
| 7.  | The sum $E$ of the potential energies in the unit cell and the corresponding Birch-Murnaghan fit. In comparison with figure 6b $\sigma_{\text{init}}$ is changed to $\sigma_{\text{mod}}$ . . . . .  | 11 |
| 8.  | Calculated diffraction pattern for 350 K. . . . .  | 13 |
| 9.  | Region of interest of $\theta_{\text{max}} = 30$ mrad at 350 K . . . . .   | 14 |
| 10. | Schematic overview of the components of a TEM and a sketch of the convergence angle.   | 15 |
| 11. | Time development of the mean square displacement $\langle u \rangle$ at various temperatures $T$ . . . . .   | 16 |
| 12. | Temperature development of the arithmetic mean $\langle \bar{u} \rangle$ . The arithmetic mean $\langle \bar{u} \rangle$ of the mean square displacements $\langle u \rangle$ was taken from time $t_0 = 250$ ps to $t_1 = 5000$ ps for all considered temperatures. $\langle u \rangle$ is depicted in figure 11 for the temperatures $T = 5$ K, 100 K, 200 K, 290 K and 350 K. . . . . | 17 |
| 13. | Integrated Bragg intensities at temperatures between 5 and 300 K . . . . .   | 18 |
| 14. | Comparison of $I_{\text{TDS}}$ and the mean square displacement $\langle \bar{u} \rangle$ at different temperatures. . . . .   | 20 |

## List of Tables

|    |   |    |
|----|---|----|
| 1. | Values of the ratio of TDS to Bragg intensity for temperatures between 290 and 300 K. . . . . | 19 |
|----|---|----|

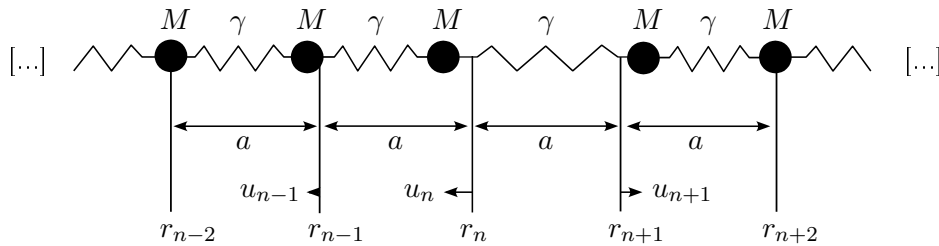


**Figure 1:** Infinite chain of atoms of mass  $M$ , spring constant  $\gamma$  and lattice parameter  $a$ .

## 1. Introduction

Gadolinium-157 exhibits a substantial magnetocaloric effect around its magnetic transition temperature of about  $20^\circ\text{C}$ . The temperature of the specimen is naturally one of the quantities one is interested in to measure when observing this process. With recent advances in electron microscopy which increased the resolution up to atomic resolution the question arises if it is possible to measure temperature down to atomic resolution. A first step to address this question is to see if it is possible in general to determine the specimen temperature from an electron diffraction image and to which degree of accuracy. Numerical calculations and simulations are presented in this project report in order to find an answer to these questions.

## 2. Theory

Selected aspects of theoretical background needed to understand the following sections is developed in this section.

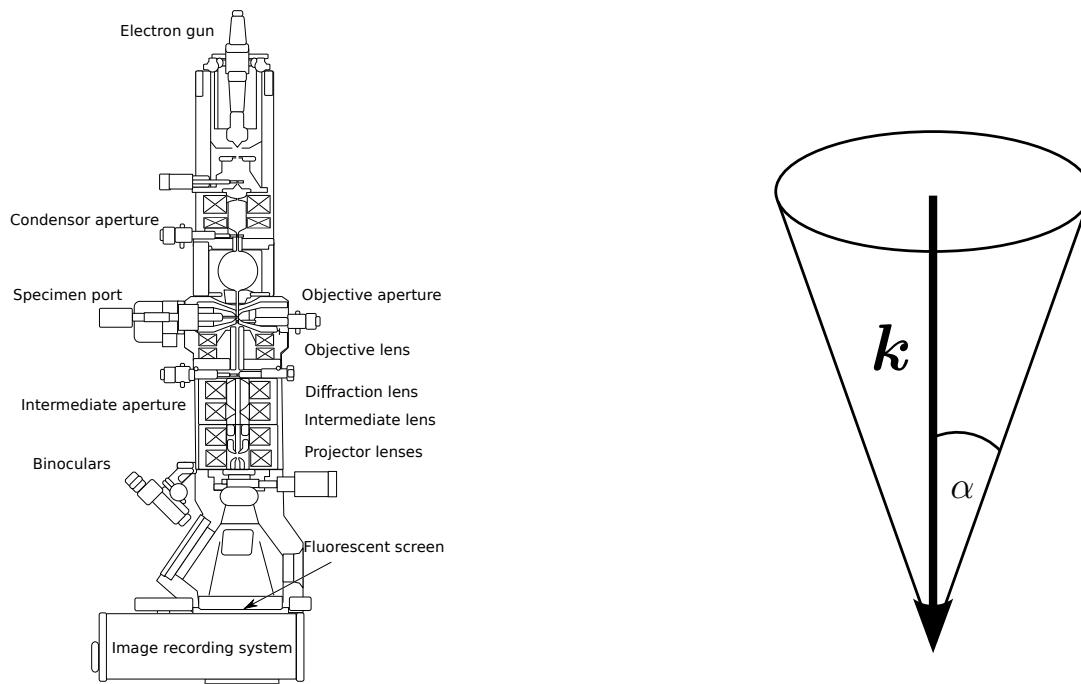
### 2.1. Lattice vibrations

A crystal without impurities can be described by a three dimensional lattice of a certain symmetry and a base set of atoms which is situated at every lattice point. Equivalently a crystal may be viewed as composed of a multitude of unit cells each containing one or more lattice points. A unit cell incorporates all of the geometric information about the crystal structure.

The atoms in a crystal vibrate at a finite temperatures. Due to the bonds between the atoms the vibrations of the single atoms become coupled and collective oscillation modes arise. In one dimension a crystal may be viewed as an infinite chain of atoms as depicted in figure 1. In order to understand how the vibrations can be described classically the bonds between the atoms are regarded as springs (harmonic approximation) and the equation of motion,

$$M \frac{d^2 u_n}{dt^2} = -\gamma (u_n - u_{n-1}) + \gamma (u_{n+1} - u_n), \quad (1)$$

is solved by a plane wave ansatz  $u_n = u_0 \exp(ikna - \omega t)$  where only nearest-neighbor interactions are considered.  $a$  is the spacing between the equilibrium positions  $r_n = na$  of the atoms and  $u_n = r_n(t) - r_n$



(a) Schematic overview of the different components of a TEM. [1]

(b) Wave vector cone around the wave vector  $k$ , perpendicular to the specimen, due to the convergence angle  $\alpha$ .

**Figure 2:** Schematic overview of the components of a TEM and a sketch of the convergence angle.

is the displacement from these at time  $t$ . The ansatz leads to a dispersion relation:

$$\omega(k) = 2\sqrt{\frac{\gamma}{M}} \sin\left(\frac{ka}{2}\right) \quad (2)$$

For a finite chain of  $N$  atoms only wave vectors  $k_m = \frac{2\pi m}{N \cdot a}$ ,  $m = 0, \pm 1, \pm 2, \dots, N/2$  are allowed.

In a quantum mechanical description each of the atoms is oscillating in a harmonic potential which gives to certain allowed oscillation mode and energy eigenstates. The quantized excitations (quasiparticles) of these quantum mechanical oscillators are called phonons. They act in scattering processes as if they had momentum  $\mathbf{p} = \hbar\mathbf{k}$ .

## 2.2. Transmission electron microscopy

The transmission electron microscope (TEM) is a imaging device which probes the specimen by exploiting the electron's quantum mechanical wave nature. In contrast to a reflection electron microscope a TEM measures the electrons which have passed through the specimen rather than measuring the electrons reflected by the sample. A schematic overview of a TEM is depicted in figure 2a. The electron beam gets accelerated to an energy of commonly 60 keV - 400 keV by an electron gun, focussed by a system of electrostatic and magnetic lenses and passes then through the specimen. Behind the sample the electrons get collected by a detector which is nowadays usually a CCD camera.

## Image formation

The two main components responsible for the formation of the electron diffraction pattern of crystals, Bragg and thermal diffuse scattering, are presented in this section. The TEM is capable of producing images for various other types of specimen including biomaterials, molecules and small animals such as ants but this is of no importance for this project and will not be regarded here. The atoms of a crystal are situated periodically in real (coordinate) space. Each of the atoms posses an electrical field which spreads into the surrounding space. Electrons incident on a crystal surface interact with the electric fields and get scattered. Due to the electron's wave nature the scattered waves can interfere constructively and destructively. This is analogous to the diffraction of X-rays on crystals but the wave lengths of electrons are much smaller in comparison (see section 2.5). In addition to that the Bragg law holds true for transmission electron microscopy:

$$2 \sin(\theta_{B,n}) = \frac{n \cdot \lambda}{d} \quad (3)$$

where  $\theta_B$  is the Bragg angle,  $\lambda$  the electron's wave length,  $d$  the distance between two lattice planes and  $n \in \mathbb{Z}$ . Therefore one sees so called Bragg spots where the scattering angle  $\theta$  equals twice the Bragg angle  $\theta_B$ .

As one considers thermal vibrations in the crystal the electron intensity in the domains between the Bragg spots becomes non zero. This effect appears because of the thermal diffuse scattering (TDS), the scattering of electrons due to the thermal vibrations of the specimen. In this case the atoms are constantly moving and with them their electric potentials which give rise to electron scattering. Thus the intensity behind the crystal is not only a function of the spacial coordinates anymore but it becomes time dependent and electrons can be scattered into regions which do not comply with the Bragg law. But the intensity due to Bragg scattering does not disappear as soon as thermal vibrations are switched on. For temperatures well below the melting point the atoms oscillate around their equilibrium position and the probability to measure it has still a maximum at this position. This gives rise to continued Bragg scattering with a lower intensity.

The resolution of the electron microscope is of course limited. Neglecting aberrations of the electromagnetic lenses the resolution limit can be calculated from the Airy formula:

$$\theta_{\text{res}} \approx 1.22 \frac{\lambda}{D} \quad (4)$$

where  $\theta_{\text{res}}$  is the smallest angle which can be resolved,  $\lambda$  is the wave length and  $D$  the diameter of the electron microscope aperture. In fact the lenses and the focus of the electron beam have the same effect as a diffracting aperture.

## Convergence angle

In some cases such as atomic resolution microscopy it is desirable to use a convergent electron beam instead of parallel illumination of the specimen. This means that the wave vectors  $\mathbf{k}$  of the incident electrons form a cone as shown in figure 2b. The angle  $\alpha$  is called convergence angle and can be tuned in experiments. It is usually very small with a magnitude of the order of a few mrad. Note that the

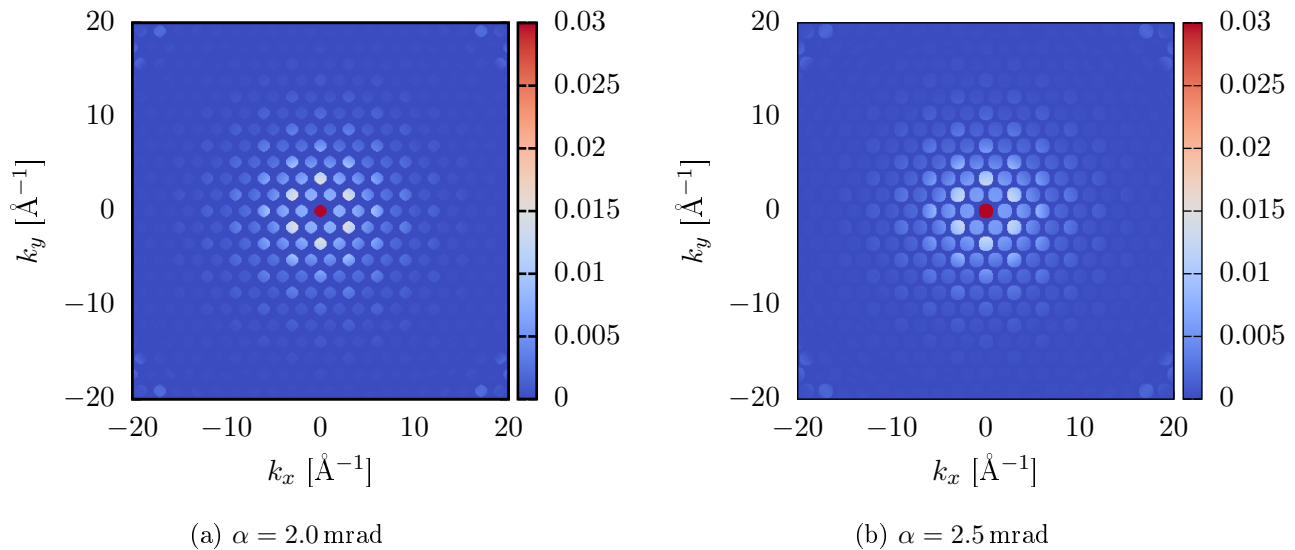


**Figure 3:** Comparison of excerpts of a computer simulated diffraction pattern in reciprocal space with different convergence angles  $\alpha$  without thermal vibrations. The colors encode the magnitude of the electron's wave function's probability amplitude  $\sqrt{|\Psi|^2}$

angle depicted in figure 2b is greatly exaggerated. For a convergent beam these spots become discs of a finite radius in reciprocal space. The relation between  $k_{r,\text{disc}}$  and  $\alpha$  reads:

$$k_{r,\text{disc}} = \frac{2\pi}{\lambda} \sin(\alpha) \quad (5)$$

Computer simulated Bragg spot patterns with a finite radius in reciprocal space are pictured in figure 3. one clearly notices that a larger convergence angle leads to a larger radius  $k_{r,\text{disc}}$ .

### 2.3. Fast electron approximation of the Schrödinger equation

In Quantum Mechanics an electron is described by a wave function which propagates through space. The electron encounters electrostatic fields inside the crystal in a frozen phonon approximation. The interaction with the magnetic fields of the objective lenses of the TEM are neglected.

The Schrödinger equation of an electron of relativistic mass  $m = \gamma m_e$ , charge with magnitude  $e$  and kinetic energy  $E_{\text{kin}}$  in an electrostatic potential  $V(\mathbf{r})$  reads:

$$\left[ \frac{\hbar^2}{2m} \nabla^2 - eV(\mathbf{r}) \right] \Psi_f(\mathbf{r}) = E_{\text{kin}} \cdot \Psi_f(\mathbf{r}) \quad (6)$$

where  $\Psi(\mathbf{r})$  denotes the wave function. The energies in a TEM are generally of the order of several hundred keV while the kinetic energy changes due to the potential  $V(\mathbf{r})$  are in general of the order of eV as long as only forward scattering is considered. The scattering potential of each atom diverges in the immediate vicinity of the atomic core but electrons which scatter into this region are mostly scattered to very large angles or even backscattered. Therefore one is able to decompose the wave function for a high energy electron travelling in  $z$ -direction into a fast oscillating,  $z$ -dependent exponential and

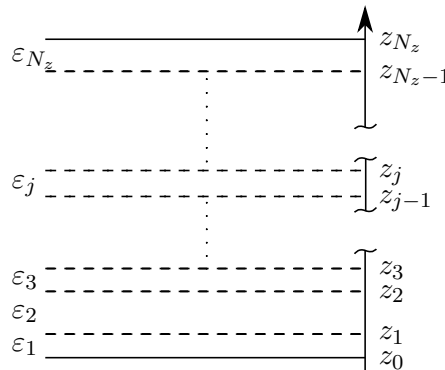


**Figure 4:** Schematic drawing of the crystal slices in the multislice approach.

a slower changing function  $\phi(\mathbf{r})$  which captures the changes of the wave function  $\Psi(\mathbf{r})$  due to the potential:

$$\Psi_f(\mathbf{r}) = \Psi(\mathbf{r}) \exp(ikz) = \Psi(\mathbf{r}) \exp(i2\pi z/\lambda) \quad (7)$$

$k^2 = k_x^2 + k_y^2 + k_z^2 = \frac{4\pi^2}{\lambda^2}$  is thereby the length of the electron's wave vector and  $\lambda$  its wave length. Furthermore only elastic scattering processes will be considered and the kinetic energy may be written as

$$E_{\text{kin}} = \frac{p^2}{2m} = \frac{\hbar^2}{2m\lambda^2} \quad (8)$$

using DE BROGLIE'S equation  $\lambda = \frac{h}{p}$  for the wave length of matter particles. As shown by Kirkland equation (6) becomes after substituting  $\Psi_f$  according to equation (7) and calculating the derivatives [2, p. 128-129]:

$$-\frac{\hbar^2}{2m} \left[ \nabla_{xy}^2 + \frac{\partial^2}{\partial z^2} + \frac{4\pi i}{\lambda} \frac{\partial}{\partial z} + \frac{2meV(x, y, z)}{\hbar^2} \right] \Psi(x, y, z) = 0 \quad (9)$$

As Kirkland describes further  $\lambda$  is very small in a high energy approximation and the motion of this electron is mainly directed in the forward direction implying that  $\Psi$  changes slowly with  $z$  [2, p. 129-130]. Therefore one may write:

$$\left| \frac{\partial^2}{\partial z^2} \Psi(x, y, z) \right| \ll \left| \frac{1}{\lambda} \frac{\partial}{\partial z} \Psi(x, y, z) \right| \quad (10)$$

One neglects therefore the second derivative with respect to  $z$  in (9) and arrives at the Schrödinger equation for fast electrons:

$$\frac{\partial \Psi(x, y, z)}{\partial z} = \left[ \frac{i\lambda}{4\pi} (\nabla_{xy}^2 + \sigma V(x, y, z)) \right] \Psi(x, y, z) \quad (11)$$

where the interaction parameter  $\sigma = 2me/\hbar^2$  is used. The vector notation  $\mathbf{r}$  shall from now on be used for the spacial coordinates  $x$ ,  $y$  and  $z$ .

## 2.4. The Real Space Multislice method (RS-MS)

In order to evaluate equation (11) numerically the potential  $V(\mathbf{r})$  is sliced into thin layers of thickness  $\varepsilon_j$ ,  $1 \leq j \leq N_z$  in which the potential is taken to be a constant average (compare figure

4):

$$V_p(\mathbf{R}_j) = \frac{1}{\varepsilon_j} \frac{i\lambda}{4\pi} \int_{\sum_{i=1}^{j-1} \varepsilon_i}^{\sum_{i=1}^j \varepsilon_i} V(\mathbf{r}) dz \quad (12)$$

where  $\mathbf{R}_j$  is the set of points situated in layer  $j$  with  $z$ -coordinate  $\sum_{i=1}^{j-1} \varepsilon_i \leq z_j \leq \sum_{i=1}^j \varepsilon_i$ . This integration justifies as well the negligence of energy changes due to the scattering potential since the integral becomes even in the vicinity of the atomic core finite and of the order of typically some eV.

The solution to equation (11) at  $z = \sum_{j=1}^n \varepsilon_j$  may then be expressed as:

$$\Psi(\mathbf{R}_n) = \prod_{j=1}^n \exp \left[ \frac{i\lambda\varepsilon_j}{4\pi} (\nabla_{xy}^2 + \sigma V_p(\mathbf{R}_j)) \right] \Psi(\mathbf{R}_0) \quad (13)$$

$\mathbf{R}_0$  are the points in the  $xy$ -plane at the surface of the specimen where  $z = 0$  and the electron still posses its initial wave function  $\Psi_0 = \Psi(\mathbf{r}_0)$  produced by the optics of the TEM.

Equation (13) may be computed by an iteration over  $j$ :

$$\Psi(\mathbf{R}_n) = \exp \left[ \frac{i\lambda\varepsilon_n}{4\pi} (\nabla_{xy}^2 + \sigma V_p(\mathbf{R}_n)) \right] \Psi(\mathbf{R}_{n-1}) \quad (14)$$

$$= \exp \left[ \frac{i\lambda\varepsilon_n}{4\pi} (\nabla_{xy}^2 + \sigma V_p(\mathbf{R}_n)) \right] \exp \left[ \frac{i\lambda\varepsilon_{n-1}}{4\pi} (\nabla_{xy}^2 + \sigma V_p(\mathbf{R}_{n-1})) \right] \dots \quad (15)$$

$$\exp \left[ \frac{i\lambda\varepsilon_j}{4\pi} (\nabla_{xy}^2 + \sigma V_p(\mathbf{R}_j)) \right] \dots \exp \left[ \frac{i\lambda\varepsilon_1}{4\pi} (\nabla_{xy}^2 + \sigma V_p(\mathbf{R}_1)) \right] \Psi(\mathbf{R}_0), \quad (16)$$

In a next step the exponentials are expanded:

$$\Psi(\mathbf{R}_j) = \sum_{m=0}^{\infty} \frac{1}{m!} \left[ \frac{i\lambda\varepsilon_j}{4\pi} (\nabla_{xy}^2 + \sigma V_p(\mathbf{R}_j)) \right]^m \Psi(\mathbf{R}_{j-1}). \quad (17)$$

Let now  $\Psi_{m-1} = \frac{1}{(m-1)!} \left[ \frac{i\lambda\varepsilon_j}{4\pi} \right]^{m-1} (\nabla_{xy}^2 + \sigma V_p(\mathbf{R}_j))^{m-1}$ , which leads to a second recursion formula

$$\begin{aligned} \Psi_m &= \frac{1}{m} \left[ \frac{i\lambda\varepsilon_j}{4\pi} \right] (\nabla_{xy}^2 + \sigma V_p(\mathbf{R}_j)) \Psi_{m-1} \\ &= \frac{1}{m} \left[ \frac{i\lambda\varepsilon_j}{4\pi} \right] \left( \frac{\partial^2}{\partial x^2} + \frac{\partial^2}{\partial y^2} + \sigma V_p(\mathbf{R}_j) \right) \Psi_{m-1} \end{aligned} \quad (18)$$

The second order derivatives can be calculated via a so called three-, five-, seven-, or nine-point-method where the higher numbered method provides a better accuracy than a lower numbered one [3, p. 314-315]. The code used in this project utilizes the 5-point method. In numerical simulations the wave functions  $\Psi_m$  are represented by their discrete values  $\Psi_m(n_x, n_y)$  on a  $xy$ -grid of size  $N_x \times N_y$ .  $n_x$ ,  $n_y$ ,  $N_x$  and  $N_y$  are integers. Furthermore it is  $1 \leq n_x \leq N_x$  and  $1 \leq n_y \leq N_y$ . The five point method approximates the second derivative with respect to  $x$  as:

$$\frac{\partial^2}{\partial x^2} \Psi_m(n_x, n_y) = \frac{1}{\Delta x^2} \left[ \frac{4}{3} \eta_{x,1} - \frac{1}{12} \eta_{x,2} \right] \quad (19)$$

where  $\eta_{x,k} = \Psi_{m-1}(n_x + k, n_y) + \Psi_{m-1}(n_x - k, n_y) - \Psi_{m-1}(n_x, n_y)$ ,  $k = 1, 2$ . This holds as well true for the derivative in  $y$  direction where  $\eta_{x,k} \rightarrow \eta_{y,k} = \Psi_{m-1}(n_x, n_y + k) + \Psi_{m-1}(n_x, n_y - k) - \Psi_{m-1}(n_x, n_y)$  and  $\Delta x^2 \rightarrow \Delta y^2$  [3, p. 315].

The iteration formulas described above can be easily solved by a computer. One just needs to specify a criterion at which order  $m = m_{max}$  the higher order terms are small enough to be neglected and one needs to know the incident wave function  $\Psi(\mathbf{R}_0)$  as well as the potential  $V(\mathbf{r})$ .

## 2.5. Frozen phonon approximation

According to equation (2) the maximum acoustical phonon frequency  $\omega$  is given by:

$$\omega = 2\sqrt{\frac{\gamma}{m}} \quad (20)$$

where the force constant  $\gamma$  may be estimated from Young's modulus  $Y$ :

$$Y = \frac{\gamma}{a} \quad (21)$$

$$\Rightarrow \omega = 2\sqrt{\frac{Ya}{m}} \quad (22)$$

For Gadolinium it is:  $a = 3.636 \text{ \AA}$ ,  $Y = 54.8 \text{ GPa}$  and  $m = 157.14 \text{ u}$ . This results in a maximum phonon frequency of  $\omega = 1.804 \cdot 10^{13} \text{ s}^{-1}$  which complies to a time of

$$\tau = \frac{2\pi}{\omega} = 3.483 \cdot 10^{-13} \text{ s} \quad (23)$$

for one atom oscillation. An electron with rest energy  $R = 511 \text{ keV}$  accelerated to a kinetic energy  $E_{kin} = 300 \text{ keV}$  travels with a speed

$$\begin{aligned} v &= c\sqrt{1 - \frac{R^2}{(R + E_{kin})^2}} \\ &= 2.328 \cdot 10^8 \text{ m s}^{-1} \\ &\approx 0.78 \cdot c \end{aligned} \quad (24)$$

in the laboratory system. It passes through a specimen of thickness  $d = 30 \text{ nm}$  in a time

$$t = \frac{d}{v} = 1.289 \cdot 10^{-16} \text{ s}.$$

Therefore one atom oscillates  $\frac{t}{\tau} = 7.14 \cdot 10^{-4}$  times while the electron passes through the specimen. As a result the change of the electric potential during one pass of an electron is negligible especially since the maximum phonon frequency has been used to obtain above estimations and the modes of this frequency are only excited at high temperatures.

Furthermore the time which elapses between two consecutive beam electrons is very small compared to the time of one oscillation. A customary Cold FEG electron gun has a current density  $J \approx 10^6 \text{ A m}^{-2}$  at  $100 \text{ keV}$  [4, p. 74]. Assuming that this current density incides on a  $A_{simcell} = 60 \text{ \AA} \times 60 \text{ \AA}$  big area

of the crystal (one simulation cell, compare chapter 3.1) the electron intensity  $I$  of the sample can be computed as:

$$I = J \cdot \frac{A_{\text{simcell}}}{e} \approx 2 \cdot 10^8 \text{ s}^{-1}$$

where  $e = 1.602 \cdot 10^{-19} \text{ C}$  is the charge of an electron. Thus  $\frac{\omega}{I} \approx 10^5$  is the average number of oscillations of one atom between two consecutive electrons. In reality the beam gets focused and the actual intensity may not be calculated from illuminated area but nevertheless the calculation as presented here gives a rough estimation of the involved time scales. Overall this justifies the approximation to simulate the diffraction pattern of snapshots which have a certain spacing in time from each other since the electrons do not have a high enough intensity to trace the path of an atom over time.

Therefore one may apply the so called *frozen phonon approximation* for computer simulations in which the electron beam is simulated to pass through a static snapshot of the vibrating crystal structure. The summation of several such electron propagations converges to the TEM image as it is seen in an experiment.

### 3. Method

As the frozen phonon approximation justifies, the diffraction pattern of a crystal structure can be obtained by averaging the simulation results of the propagation of an electron wave function through a static crystal structure over a multiple of different structure snapshots of the vibrating structure. These snapshots are simulated using the LAMMPS molecular dynamics software [5]. For this purpose a Lennard-Jones potential is fitted to Gadolinium such that its tabulated Bulk-modulus is reproduced. This potential is then used to calculate 100 snapshots of the vibrating crystal structure at different temperatures using Nosé-Hoover thermostat classical molecular dynamics. The snapshots are then supplied to a program which simulates the electron scattering in the structure and calculates the electron intensity distribution behind the crystal. The intensity of the Bragg spots is then integrated and compared to the integrated intensity of the TDS.

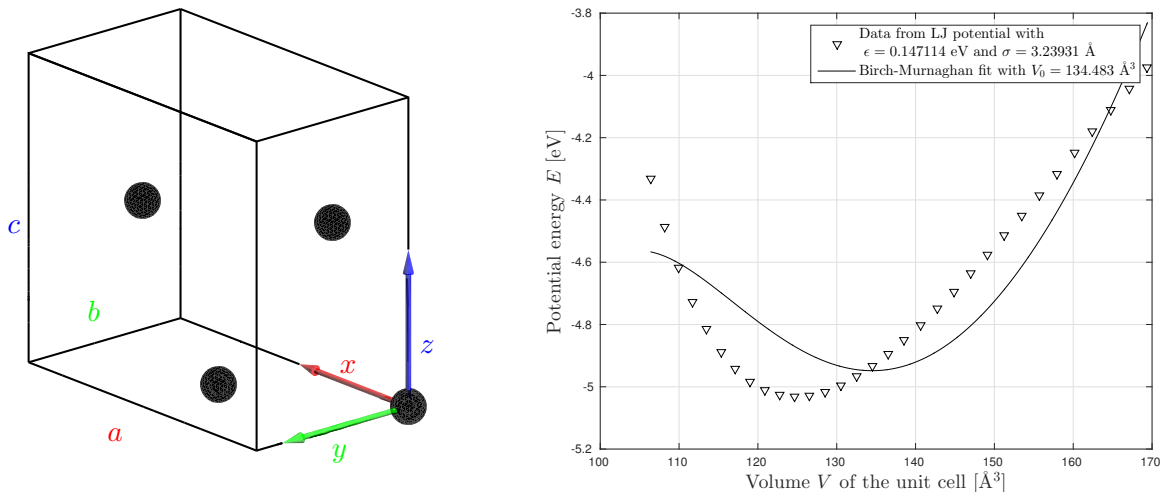
#### Obtaining a suitable atomic interaction potential for a gadolinium-like, perfect hcp crystal structure

Gadolinium freezes at temperatures below 1585 K into a hcp crystal structure. The multislice code used to simulate the electron propagation in the specimen allows only orthorhombic simulation cells to be used. An orthorhombic unit cell of Gadolinium is depicted schematically in figure 6a. Real Gadolinium has orthorhombic unit cell parameters  $a = \sqrt{3} \cdot 3.636 \text{ \AA}$ ,  $b = 3.636 \text{ \AA}$  and  $c = 5.783 \text{ \AA}$  which do not correspond to a perfect hcp structure since

$$\frac{a}{c} = 0.6288 \leftrightarrow \frac{a_{\text{perfect}}}{c_{\text{perfect}}} = 0.6124. \quad (25)$$

In order to simulate thermal vibrations one needs a model for an interatomic potential. Since there is no tabulated interatomic potential for Gadolinium available in LAMMPS a Lennard-Jones (LJ) potential,

$$U(r) = 4\epsilon \left[ \left( \frac{\sigma}{r} \right)^{12} - \left( \frac{\sigma}{r} \right)^6 \right], \quad (26)$$



(a) Orthorhombic unit cell of the real Gadolinium hcp structure. (b) The data points of the sum  $E$  of all potential energies of all atoms per unit cell are computed by LAMMPS and the fit is calculated according to (27).  $\sigma_{\text{init}} = 2^{-1/6}b$  is set.

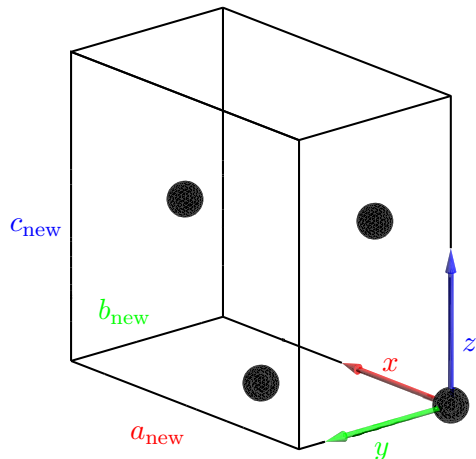
**Figure 5:** Real Gadolinium crystal structure with unit cell parameters  $a$ ,  $b$ ,  $c$  (compare text for the values) and the computed sum of the potential energies  $E$  of the atoms in one unit cell for small deviation from the expected minimum volume  $V_0$  for the real Gadolinium structure.

is fitted such that it allows a correct prediction of the experimental bulk modulus  $B_{\text{Gd}} = 38$  GPa of Gadolinium at the expected unit cell volume  $V_0 = a \cdot b \cdot c = 132.413 \text{ \AA}^3$ . In equation (26) it is  $\sigma = 2^{-1/6}r_m$ .  $r_m$  is the radius at which the potential has its minimum and  $\epsilon$  is proportional to the depth of the potential since  $U(r = r_m) = 4\epsilon$ . It is expected that  $r_m = b$  at a temperature  $T = 0\text{K}$  since this is the equilibrium distance between nearest neighbors in a hcp structure. In order to find a suitable potential  $\sigma_{\text{init}} = 2^{-1/6}b = 3.239 \text{ \AA}$  is set. Therefore one just has to determine  $\epsilon$ . To achieve that the total potential energy  $E(V)$  of a unit cell with volume  $V$  is calculated with LAMMPS for  $0.985 \cdot V_0 \leq V \leq 1.015 \cdot V_0$  with a potential cutoff distance of  $5.5\sigma$ . The resulting data is then fitted according to the Birch-Murnaghan equation of states [6, 7],

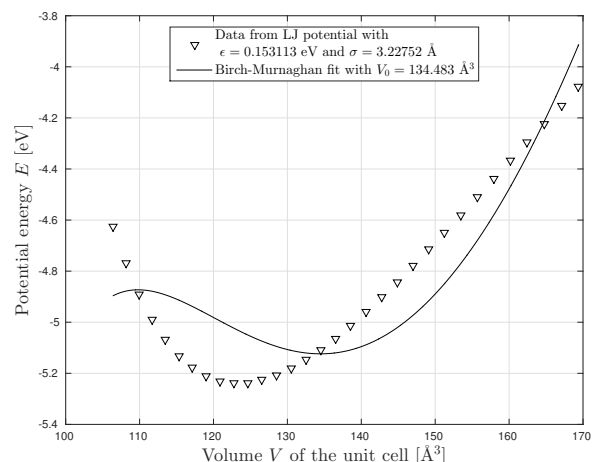
$$E(V) = E_0 + \frac{9V_0B_0}{16} \left\{ \left[ \left( \frac{V_0}{V} \right)^{\frac{2}{3}} - 1 \right]^3 B'_0 + \left[ \left( \frac{V_0}{V} \right)^{\frac{2}{3}} - 1 \right]^2 \left[ 6 - 4 \left( \frac{V_0}{V} \right)^{\frac{2}{3}} \right] \right\}, \quad (27)$$

where  $B_0$  is the bulk modulus and  $B'_0 = \left( \frac{\partial B_0}{\partial P} \right)_{P=0}$  the derivative of it with respect to the pressure  $P$  at  $P = 0$ .  $B_0$  is then compared to  $B_{\text{Gd}}$ . The MATLAB code which is used in this project is quoted in appendix A.1. The result of this process is depicted in figure 5b. It has to be mentioned that in all the calculations from here on  $V_0 = 134.483 \text{ \AA}^3$  and  $c = 5.873 \text{ \AA}$  due to a mistake in the fitting calculation code which was unfortunately discovered too late to be corrected for this report. Note that the mistake is a change of 1.5% in volume so it is highly unlikely that it has any qualitative influence on the results. The fit with minimum at  $V_0$  does not agree very well with the potential energies as calculated by LAMMPS. Note that  $\sigma = 2^{-1/6} \cdot b$  is fixed in this fit. The minimum of the data points is shifted towards a volume smaller than the expected  $V_0$ .

In order to reach a good agreement between data and fit one has to modify the input parameters of the fit procedure, either the unit cell parameters  $a$ ,  $b$  and  $c$  or  $\sigma$ , such that the calculated potential energy



(a) Orthorhombic unit cell of the modified Gadolinium hcp structure.



(b) The data points of the sum  $E$  of all potential energies of all atoms per unit cell are computed by LAMMPS and the fit is calculated according to (27) using the modified Gadolinium structure.

**Figure 6:** Modified unit cell with unit cell parameters  $a_{\text{new}}$ ,  $b_{\text{new}}$  and  $c_{\text{new}}$  (compare text for the values) as well as results of the sum  $E$  of the potential energies in the unit cell and the corresponding Birch-Murnaghan fit.  $\sigma_{\text{init}} = 2^{-1/6}b$  is kept the same as in figure 5.

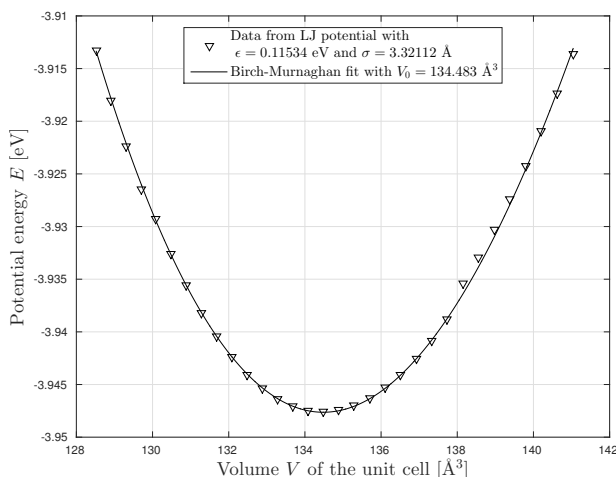
of the unit cell shows a minimum at the expected real unit cell volume  $V_0$ . The Lennard-Jones potential is radially symmetric and involves only pair interactions which in turn leads to the lowest potential energy when all the atoms are situated at the minimum distance  $r_m$  of the interatomic potential apart from each other in a tetrahedral fashion. Therefore the LJ potential leads automatically to a perfect closed packed structure such as hcp or fcc. More sophisticated models for interatomic potentials include changes due to bonding angles and shear forces but it is beyond the scope of this project to fit such a potential. Instead the crystal structure is modified such that it becomes a perfect hcp structure. In order to achieve this  $c$  has been changed to  $c_{\text{mod}} = \sqrt{\frac{8}{3}}b$ . The new lattice parameters  $a_{\text{new}}$ ,  $b_{\text{new}}$  and  $c_{\text{new}}$  are then calculated according to:

$$V_{0,\text{mod}} = a \cdot b \cdot c_{\text{mod}} \quad \Rightarrow \quad a_{\text{new}} = a \cdot (f_V)^{1/3}, \quad b_{\text{new}} = b \cdot (f_V)^{1/3}, \quad c_{\text{new}} = c_{\text{mod}} \cdot (f_V)^{1/3} \quad (28)$$

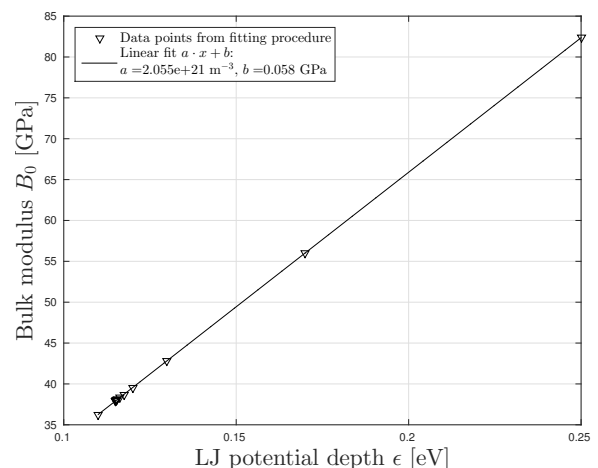
where  $f_V = \frac{V_0}{V_{0,\text{mod}}} = 0.989$ . These new unit cell parameters are used in the fit shown in figure 6b.

The modification of the unit cell to a perfect hcp structure does not suffice to reach a good agreement of the fit according to the Birch-Murnaghan equation of states with the sum  $E$  of all potential energies inside an unit cell. The second parameter of the LJ-potential,  $\sigma$ , needs to be increased by 2.9% to  $\sigma_{\text{mod}} = 1.029 \cdot 2^{-1/6} \cdot b_{\text{new}}$  in order to shift the minimum of the Birch-Murnaghan fit to  $V_0$ . This results in the fit of figure 7a. The maximum and minimum considered volume to obtain this fit are lowered compared to the fits in figure 5b and 6b since the fit gets more sensitive to the slope around the real unit cell volume. On the other hand the volumes are bigger in the other fits to show the discrepancy between the expected volume and the one calculated from the structure.

A linear relationship between  $\epsilon$  and the Bulk modulus  $B_0$  for the accepted fit is found as a side result. It is depicted in figure 7b. From knowing this one does not need to find the desired  $\epsilon$  through an iterative



(a) The data points of the sum  $E$  of all potential energies of all atoms per unit cell are computed by LAMMPS at temperature  $T = 0$  K and the fit is calculated using the modified Gadolinium structure according to (27).



(b) Linear relationship between the Bulk modulus  $B_0$  and the depth  $\epsilon$  of the LJ-potential.

**Figure 7:** The sum  $E$  of the potential energies in the unit cell and the corresponding Birch-Murnaghan fit. In comparison with figure 6b  $\sigma_{\text{init}}$  is changed to  $\sigma_{\text{mod}}$ .

procedure but it suffices to calculate the bulk modulus for two different  $\epsilon$ , connect them by a straight line and read off the sought  $\epsilon$  at the respective bulk modulus. One can safely assume that this method is valid for hcp structures in combination with a LJ interatomic potential.

### 3.1. Setting up the multislice code

The multislice code used for this project was developed at the Material's Theory group at the Physics department of Uppsala University. It allows to tune the convergence angle  $\alpha$  as it is pictured in figure 3. A convergence angle  $\alpha = 2.0$  mrad is chosen which leads to fairly round Bragg spots with a sufficient number of pixels to integrate and this choice of the angle provides at the same time enough space between the spots to integrate a sufficient number of pixels for the TDS intensity.

Furthermore a suitable simulation cell size needs to be found. The dimensions in  $x$  and  $y$  direction must be chosen such that the wave function has a sufficiently small magnitude at the borders of the cell. The thickness in  $z$ -direction should be set to a value which can easily be used in experiment. Thus the cell size is chosen to be 10 unit cells in  $x$ -, 17 in  $y$ - and 51 in  $z$ -direction which results in simulation super cell dimensions of

$$\begin{aligned} A &= 62.75 \text{ \AA} \\ B &= 61.59 \text{ \AA} \\ C &= 301.72 \text{ \AA} \end{aligned}$$

A convergence angle  $\alpha = 2.0$  mrad is chosen. The simulation cell needs furthermore to be discretized for numerical calculations which was done by introducing a grid of size  $N_x \times N_y \times N_z$

with:

$$N_x = 1250$$

$$N_y = 1225$$

$$N_z = 3009$$

### 3.2. Setting up thermal vibration simulation

In order to have a sufficiently large number of snapshots for the convergence of the multislice diffraction pattern  $N_s = 100$  snapshots are chosen to be calculated in the thermal vibration simulation by LAMMPS. The correlation between the atom positions of two consecutive snapshots should be as small as possible since the smaller the correlation the faster converges the series of diffraction patterns of one snapshot to the diffraction pattern of a vibrating crystal. Or said in a different way one needs less snapshots to reach convergence when the correlation is small. A very conservative estimation of the time after which this state is reached for Gadolinium has been used: The time  $\tau$  for one oscillation of the highest frequency in Gadolinium is about  $3 \cdot 10^{-13}$  s as seen in section 2.5 so  $\tau \propto 10^{-12}$  s for smaller frequencies. For the simulation it was now assumed that the correlation between the atom positions is sufficiently small after around 50 oscillations of one atom which leads to a time  $t_{\text{snap}} = 50$  ps between the snapshots. This estimation is very conservative as it will become apparent later.

Furthermore a time step needs to be chosen for the simulation. The time step is the amount of time that is covered by one time integration of the equations of motion in the simulation. The time step is set to be 0.01 ps which should be sufficiently small to sample even the highest frequency vibrations appropriately.

The temperature range most interesting for this project is between 290 K and 300 K because Gadolinium shows a magnetic transition at approximately 293 K. Therefore it is chosen to examine this region in temperature steps of 2 K. In addition to that the temperatures 5 K, 50 K, 100 K, 150 K, 200 K, 250 K, 280 K, 310 K and 350 K are considered. The input files for lammmps are cited in appendix A.2.

### 3.3. Integrating the TDS and Bragg spot intensity in the final diffraction pattern

A reciprocal space diffraction pattern calculated for 350 K is depicted in figure 8. It exhibits spots of greater intensity due to Bragg scattering and non zero intensity between the spots due to TDS. It will be discussed in this section how the integration of the Bragg and TDS intensities may be integrated.

First one selects a region of interest where the integration is to be performed. The maximum scattering angle  $\theta_{\text{max}}$  is chosen such that the Bragg spots are well separable from the TDS intensity since the difference in intensity between spots and TDS becomes increasingly fuzzy the bigger  $\theta$  is. The results will be discussed later for a region of interest of  $\theta_{\text{max}} = 30$  mrad which is depicted in figure 9.

The center positions of the Bragg spots in reciprocal space can be calculated according to the Bragg law under consideration of the six-fold symmetry of the Gd crystal structure; compare equation (3) where  $d = \frac{\sqrt{3}}{2} \cdot b$  is the interplanar distance of Gadolinium. The radius  $k_{r,\text{disc}}$  of the spots in reciprocal

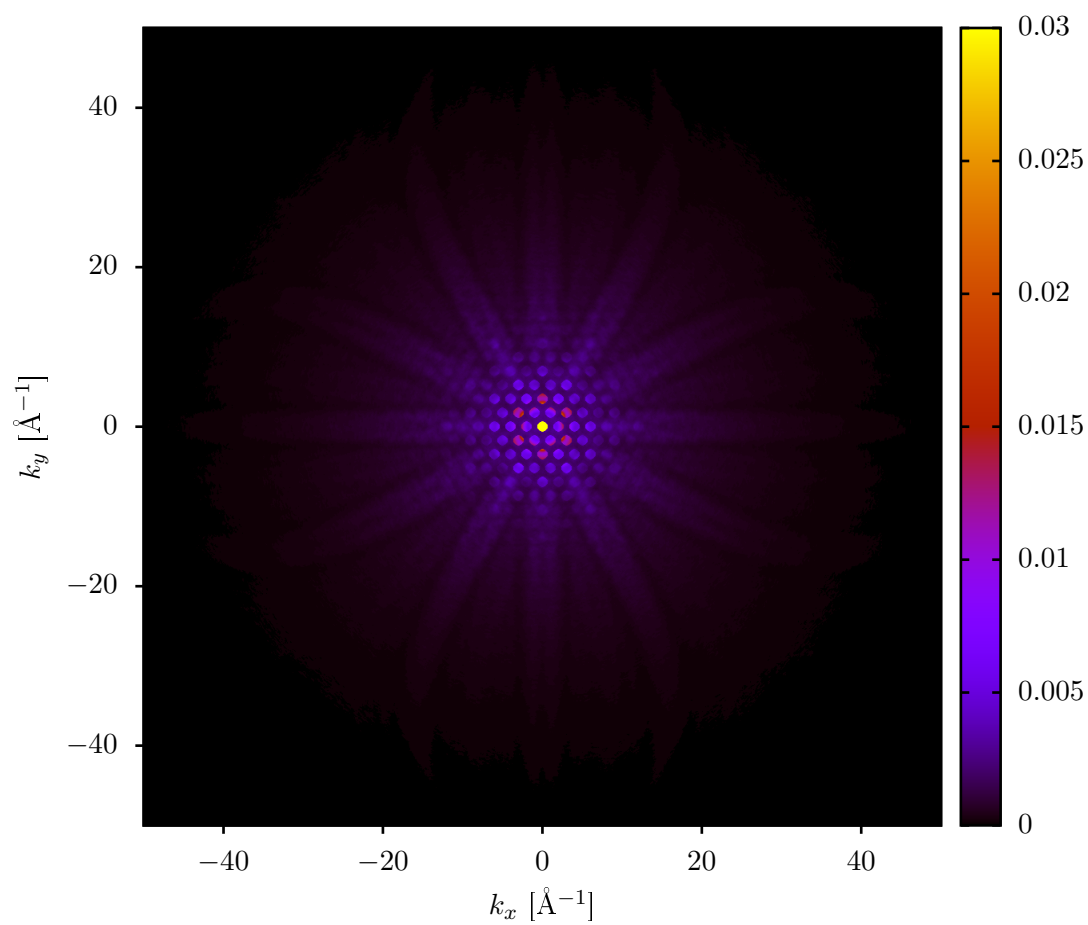


**Figure 8:** Calculated diffraction pattern for 350 K.

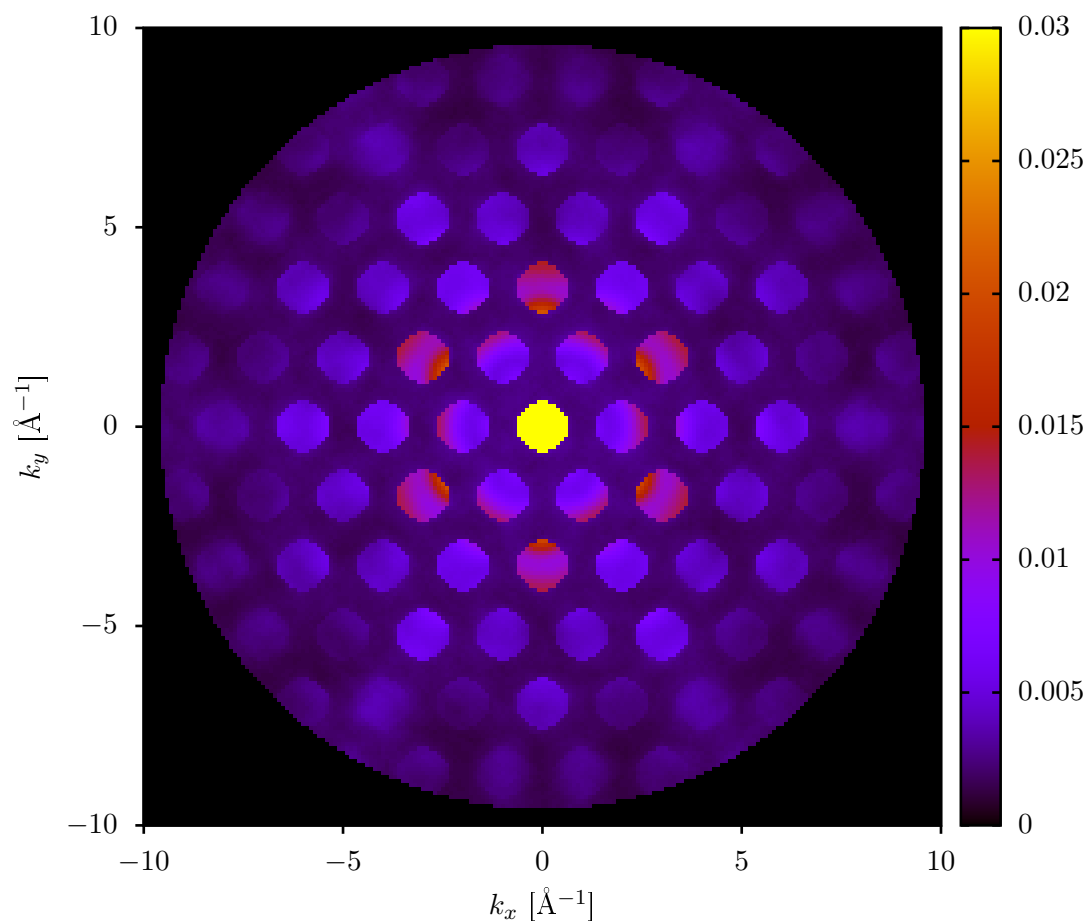


**Figure 9:** Region of interest of  $\theta_{\max} = 30$  mrad at 350 K

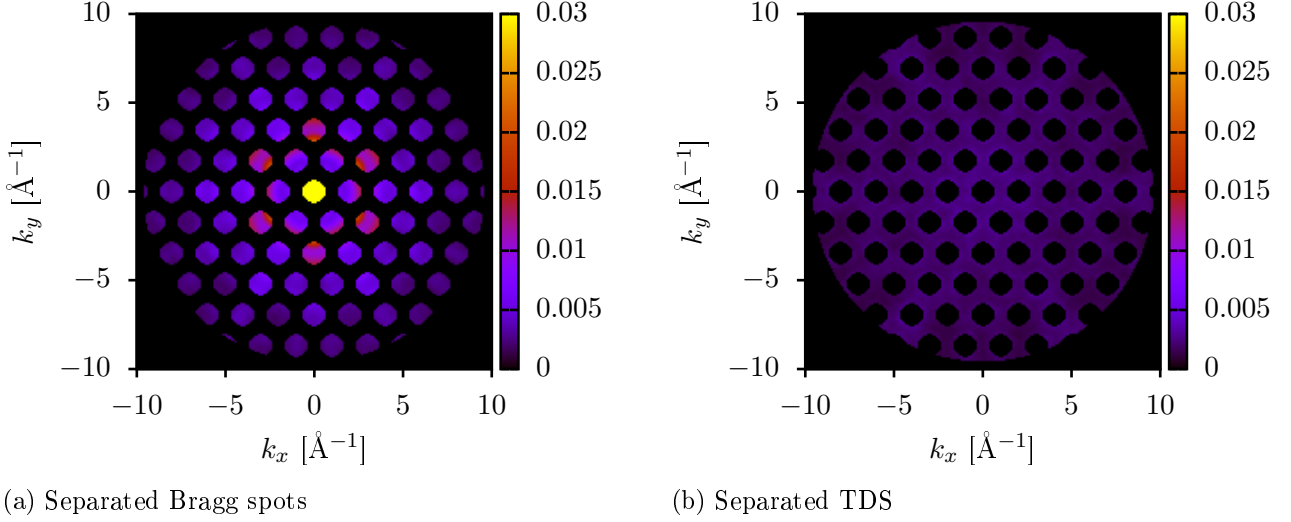


**Figure 10:** Schematic overview of the components of a TEM and a sketch of the convergence angle.

space may be computed according to equation (5). Note that the scattering angle to the  $n$ -th Bragg spot in  $x$ -direction is  $\theta_{x,n} = 2 \cdot \theta_{B,n}$ :

$$\begin{aligned}
 k_{r,\text{disc}} &= 0.638 \text{ \AA}^{-1} \\
 k_{x,n} &= k \cdot \sin(\theta_{x,n}) = k \cdot \sin(2 \cdot \theta_{B,n}) \approx k \cdot 2 \cdot \theta_{B,n} \\
 \text{for } n = 1: \quad k_{x,1} &= 2k \cdot \theta_{B,1} \approx 2k \cdot \frac{\lambda}{2d} = \frac{2\pi}{d} = \frac{4\pi}{\sqrt{3} \cdot b} = 2.003 \text{ \AA}^{-1}
 \end{aligned}$$

where only small angles  $\theta_{B,n}$  and small  $n$  are considered.  $k = \frac{2\pi}{\lambda}$  is the incoming electrons wave vector. The Separated Bragg and TDS intensities in the region of interest are depicted in figure 10 for 350 K. In order to get the Bragg or TDS intensity at one temperature the separated intensities at each grid point are added up. Note that this method does not distinguish between Bragg and TDS intensity at the Bragg spots. For a vibrating crystal structure the intensity of the Bragg spot is a sum of the intensity due to Bragg scattering and due to TDS. But the distinction between both is not possible in experiment so no further attempt to estimate the intensity of TDS at the spots is carried out.

## 4. Computational results

### 4.1. Mean square displacement of the atoms

The snapshot output files from LAMMPS contain the atom positions at certain times  $t_j$ ,  $0 \leq j \leq N_S = 100$  and  $t_j - t_{j-1} = t_{\text{snap}} = 50$  ps. The snapshot taken at  $t_0 = 0$  contains the undisturbed crystal structure without thermal vibrations. Let  $\mathbf{r}_i(t_j)$  be the position vector of the  $i$ -th atom at time  $t_j$  and  $\mathbf{u}_i(t_j) = \mathbf{r}_i(t_j) - \mathbf{r}_i(t_0)$  the displacement from its equilibrium position. Due to the use of periodic boundary conditions atoms at the borders of the simulation cell may leave the cell and reenter it on

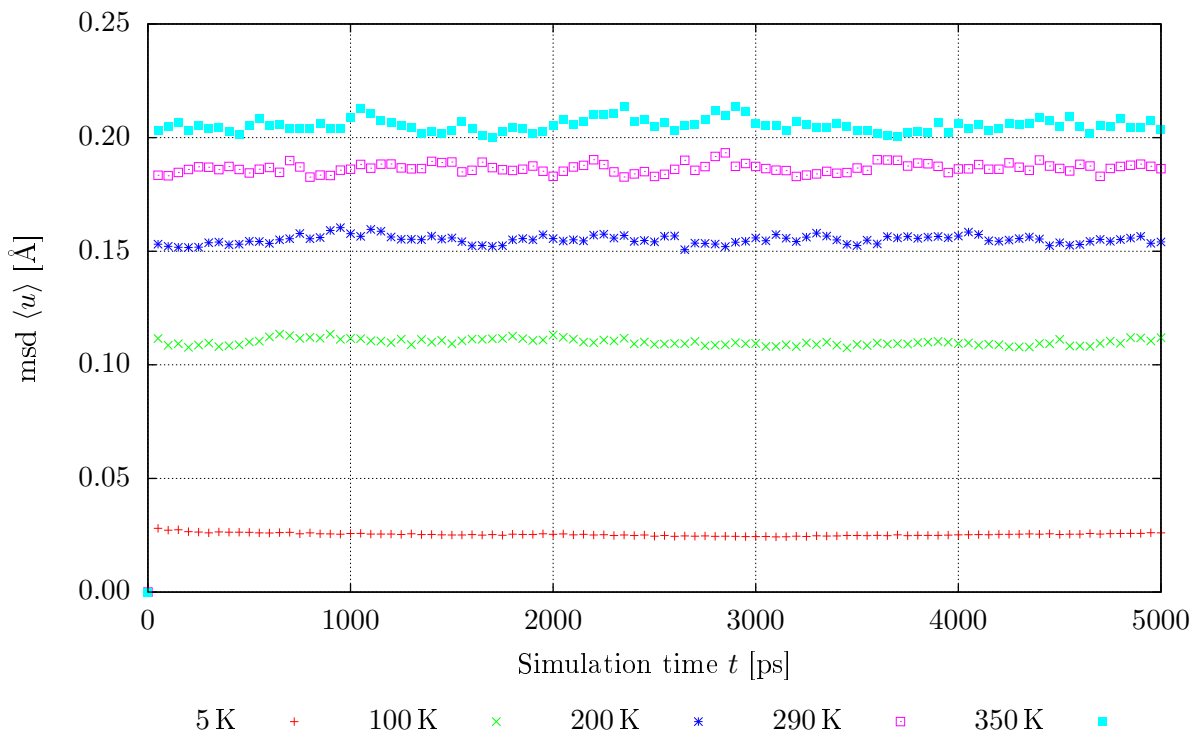


**Figure 11:** Time development of the mean square displacement  $\langle u \rangle$  at various temperatures  $T$ .

the exact opposite side. In this case the displacement is by about one length, width or thickness of the simulation cell too large and it needs to be corrected. This is done by checking the displacements for every snapshot and compare them to the super cell parameters. If in one dimension the displacement is larger than  $1/2$  of the corresponding dimension of the super cell  $A$ ,  $B$  or  $C$  the displacement gets corrected:

$$\begin{aligned} \left[ \mathbf{u}(t_j) > \frac{1}{2} (A, B, C)^\top \right] &= \mathbf{c} \\ \mathbf{u}(t_j) &= \mathbf{u}(t_j) - [\mathbf{c} \otimes (A, B, C)^\top] (1, 1, 1)^\top \end{aligned} \quad (29)$$

which is to be understood in a programming language way.  $\otimes$  denotes here the outer product and  $>$  the row-wise comparison between the involved vectors resulting in a vector  $\mathbf{c}$  containing a 1 in rows where the comparison yields true and 0 where it faults. After this correction one can compute the mean square displacement  $\langle u(t_j) \rangle$ :

$$\langle u(t_j) \rangle = \frac{1}{N_A} \sqrt{\sum_{i=1}^{N_A} (\mathbf{u}_i(t_j))^2} \quad (30)$$

where  $N_A$  is the number of atoms in the simulation cell and  $(\mathbf{u}_i(t_j))^2 = \mathbf{u}_i^\top(t_j) \mathbf{u}_i(t_j)$ . The time development of  $\langle u \rangle$  is depicted in figure 11.

The mean square displacement of the atoms of one snapshot is up to some fluctuations constant in time as one expects. The fluctuations of the mean square displacement increase with higher temperature but they do not become unreasonably big. They do not seem to be totally uncorrelated, however, as

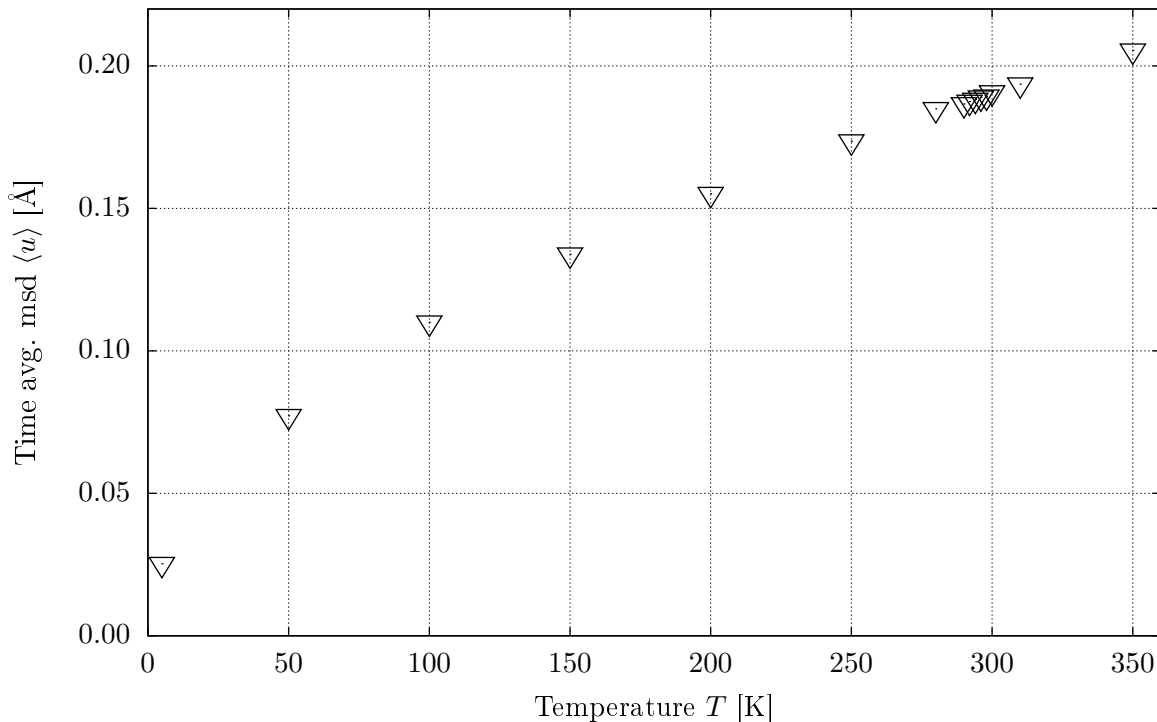


**Figure 12:** Temperature development of the arithmetic mean  $\langle \bar{u} \rangle$ . The arithmetic mean  $\langle \bar{u} \rangle$  of the mean square displacements  $\langle u \rangle$  was taken from time  $t_0 = 250$  ps to  $t_1 = 5000$  ps for all considered temperatures.  $\langle u \rangle$  is depicted in figure 11 for the temperatures  $T = 5$  K, 100 K, 200 K, 290 K and 350 K.

one would expect since a lot of the consecutive mean square displacements  $\langle u(t_l) \rangle$ ,  $l > j$ , of a mean square displacement  $\langle u(t_j) \rangle$  which is bigger than the average over all times are in turn as well bigger than the time average. Yet, the time step of 50 ps is a good choice since the mean square displacements are from 50 ps on more or less constant and all the equilibrating processes have been completed by that time.

For the comparison with the diffraction pattern the average  $\langle \bar{u} \rangle$  over time is of interest since the final diffraction pattern is the average of the diffraction patterns of the individual snapshots. It was decided to use the last 96 out of the 100 snapshots calculated by LAMMPS to compute the final diffraction pattern because this utilizes the cluster nodes most efficiently. Therefore the average was taken over times  $t_5 \leq t \leq t_{N_s}$ :

$$\langle \bar{u} \rangle = \frac{1}{N_s} \sum_{j=5}^{N_s} \langle u(t_j) \rangle \quad (31)$$

The time averaged mean square displacement is pictured in figure 12 for the considered temperatures. It increases sharply at low temperatures and continues to grow at high temperatures with a decreasing derivative. For temperatures between 290 and 300 K the time averaged mean square exhibits a monotonic increase suggesting that it is possible to map the time averaged mean square displacement to the temperature of the sample. In the next section it is discussed how this translates to the TDS intensity in the diffraction pattern.

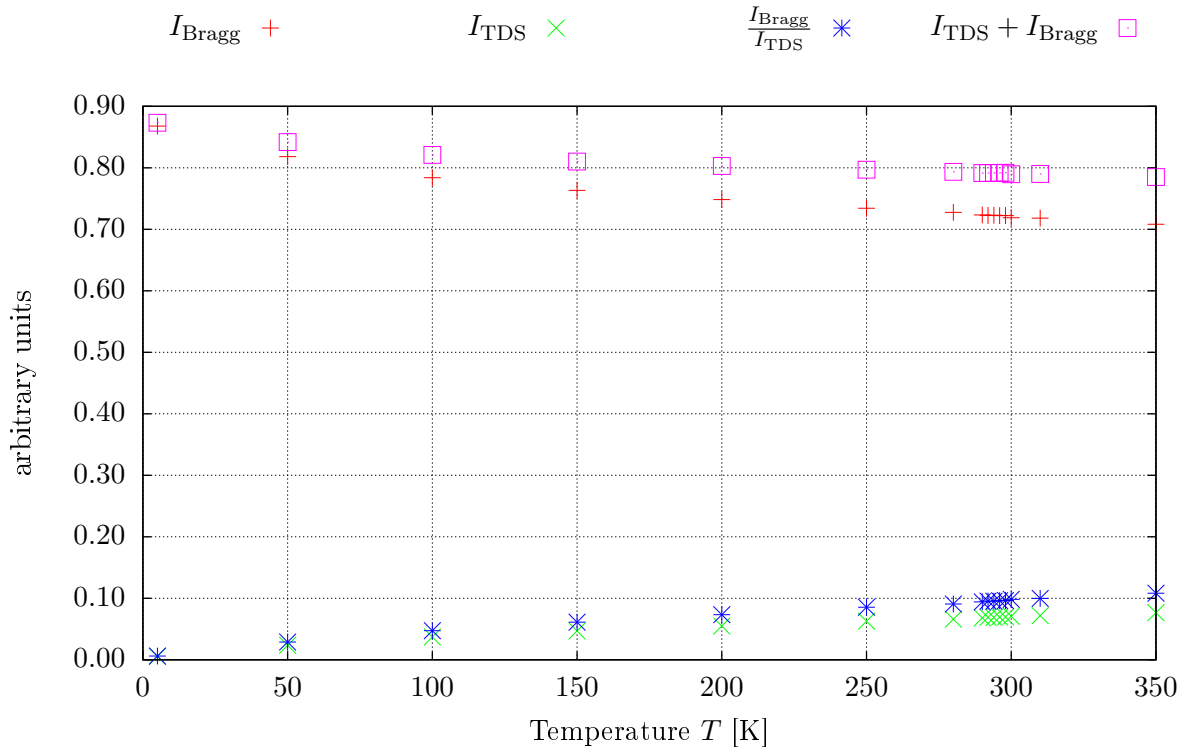


**Figure 13:** Integrated Bragg intensities at temperatures between 5 and 300 K

#### 4.2. Comparison of the intensity of the Bragg scattering with thermal diffuse scattering

The integration as described in section 3.3 yields the intensities due to Bragg scattering and TDS as depicted in figure 13 in the region of interest of maximum scattering angle  $\theta_{\max} = 30$  mrad. Generally the overall intensity due to Bragg scattering decreases with temperature whereas the overall TDS intensity increases. The absolute value of the slope of both intensities decreases with temperature exhibiting a bigger change at lower temperatures. The ratio  $\frac{I_{\text{TDS}}}{I_{\text{Bragg}}}$  of TDS to Bragg scattering increases as well with temperature. It exhibits a behavior similar to the TDS intensity. The sum  $I_{\text{TDS}} + I_{\text{Bragg}}$  of the overall intensities due to TDS and Bragg scattering decreases in the region of interest with higher temperatures.

## 5. Discussion

As depicted in figure 13 the ratio of TDS to Bragg scattering intensity is monotonically increasing in the region between 290 and 300 K. Therefore one expects to be able to map a certain value of the ratio to a temperature. The numerical values of  $\frac{I_{\text{TDS}}}{I_{\text{Bragg}}}$  displayed in table 1.

Except for the value at 294 K the ratio  $\frac{I_{\text{TDS}}}{I_{\text{Bragg}}}$  of TDS and Bragg scattering increases monotonously. Thus a mapping of  $\frac{I_{\text{TDS}}}{I_{\text{Bragg}}}$  to a temperature is possible. As it is tabulated one needs to be able to measure the ratio of TDS to Bragg scattering intensity up to a precision of about  $10^{-4}$  in order to be

able to distinguish between temperatures which differ by 2 K in the temperature range between 290 and 300 K.

**Table 1:** Values of the ratio of TDS to Bragg intensity for temperatures between 290 and 300 K.

| $T$   | 290 K | 292 K | 294 K | 296 K | 298 K | 300 K |
|---|-------|-------|-------|-------|-------|-------|
| $\frac{I_{\text{TDS}}}{I_{\text{Bragg}}} [10^{-2}]$ | 9.415 | 9.546 | 9.512 | 9.611 | 9.637 | 9.832 |

For low temperatures the precision in the measurement of  $\frac{I_{\text{TDS}}}{I_{\text{Bragg}}}$  does not need to be as accurate as for higher temperatures since the slope of  $\frac{I_{\text{TDS}}}{I_{\text{Bragg}}}$  is bigger (compare figure 13).

For higher temperatures the total electron scattering intensity  $I_{\text{TDS}} + I_{\text{Bragg}}$  decreases in the region of interest as depicted in figure 13. Thus more electrons get scattered into regions of reciprocal space corresponding to bigger scattering angles at higher temperatures. This suggests that there might be as well a way to determine the temperature from the annular dark field (ADF) image. This is not done in this project but might be subject to further research.

Furthermore the behavior of the ratio  $\frac{I_{\text{TDS}}}{\langle \bar{u} \rangle}$  with respect to the temperature  $T$  is examined and is depicted in figure 14. At low temperatures the slope of  $\frac{I_{\text{TDS}}}{\langle \bar{u} \rangle}$  is very steep and decreases sharply as the temperature gets higher. Above temperatures of about 150 K the ratio seems to saturate or at least the dependency of  $\frac{I_{\text{TDS}}}{\langle \bar{u} \rangle}$  on the temperature becomes more linear with a much smaller slope than at lower temperatures. This might give a hint how the TDS intensity depends on the mean square deviation. Further research might yield an analytical or empirical relation between those quantities.

To conclude this section it should be noted that the qualitative behavior of  $I_{\text{Bragg}}$ ,  $I_{\text{TDS}}$ ,  $\frac{I_{\text{TDS}}}{I_{\text{Bragg}}}$  and  $\langle \bar{u} \rangle$  with respect to temperature is expected to be generalizable to other materials since the specificities of the crystal structure are only taken into consideration to obtain an interaction potential and to integrate the electron scattering intensities and they should not influence the qualitative results shown in figure 13 and 14. The numerical results will differ of course.

## 6. Conclusion

The calculations done for this project show that if the necessary precision of the determination of  $\frac{I_{\text{TDS}}}{I_{\text{Bragg}}}$  of about  $10^{-4}$  is achievable in experiment it will be possible to map electron diffraction intensities to temperatures up to a precision of about  $\pm 2$  K. Starting points and question which might be subject of further research are found as well. Experiments may now check the predictions done here.

The mistake done during the fitting of the interatomic potential is not expected to have an extremely big influence on the qualitative outcomes of this project but the calculations will be done again with the correct values for a future publication.

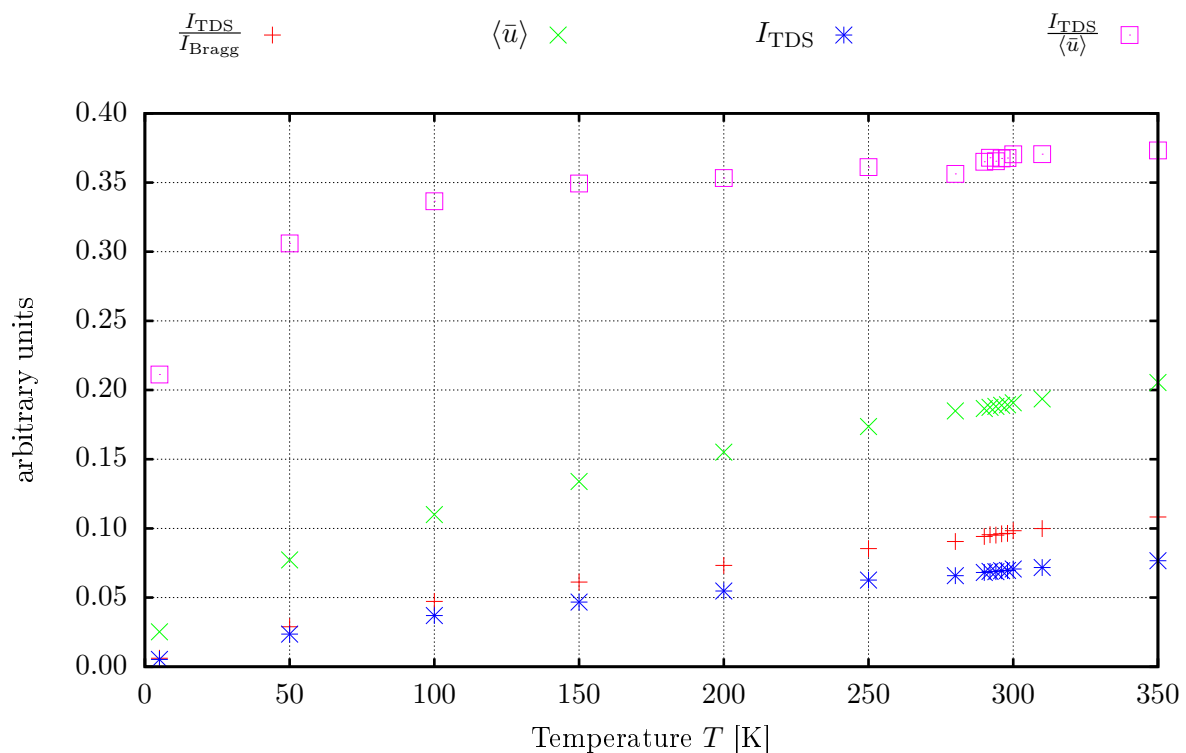


Figure 14: Comparison of  $I_{\text{TDS}}$  and the mean square displacement  $\langle \bar{u} \rangle$  at different temperatures.

## 7. Prospect

All the calculations presented here are based purely on classical physics. One further step might be to include zero-point vibrations. These nuclear quantum effects are expected to have a great influence on the mean square displacements especially at lower temperatures. Furthermore one can examine the possibility of determining the temperature by measuring the annular dark field intensity and compare this to the method described in this report. One could as well do further deliberations regarding an analytical or empirical relationship between the mean square displacement and the TDS intensity.

From an experimental point of view this might be the first step towards new kinds of research which can be addressed by electron microscopes since it is not possible to determine the temperature of the specimen until today. Questions such as the magnitude of the heating of the specimen due to the electron beam can be imagined to be regarded.

---

## References

- [1] Wikipedia: Schematic drawing of a TEM [Internet]. Cited 2015 August 21. Available from: [https://en.wikipedia.org/wiki/Transmission\\_electron\\_microscopy#/media/File:Scheme\\_TEM\\_en.svg](https://en.wikipedia.org/wiki/Transmission_electron_microscopy#/media/File:Scheme_TEM_en.svg)
- [2] Earl J. Kirkland: *Advanced Computing in Electron Microscopy*, Second ed. (Springer, New York, 2010).
- [3] Can Ying Cai, Song Jun Zeng, Hong Rong Liu, Qi Bin Yang: *Computational comparison of the conventional multislice method and the real space multislice method for simulating exit wavefunctions*, *Micron*, **40**, 313–319 (2009).
- [4] David B. Williams, C. Barry Carter: *Transmission Electron Microscopy*, Second ed. (Springer, New York 2009)
- [5] Sandia National Laboratory: LAMMPS Molecular Dynamics Simulator, version 9 Dec 2014 [Internet]. Cited 2015 August 18. Available from: <http://lammps.sandia.gov/>
- [6] Murnaghan, F. D. . *The Compressibility of Media under Extreme Pressures*. *Proc. N. A. S.*, **30** (9), 244–247 (1944)
- [7] Birch, Francis: *Finite Elastic Strain of Cubic Crystals*, *Phys. Rev. Lett.*, **71** (11), 809 (1947).

## A. LAMMPS input files

### A.1. Optimisation of the Lennard-Jones potential

Following MATLAB code has been used to obtain suitable  $\epsilon$  for the Lennard-Jones potential:

```

-----fit_potential.m-----

fitPotentiallog = fopen('fitPotential.log','w');

% Used natural constants; mass m of a Gadolinium atom
m = 157.14*1.660538921*10^(-27);
e = 1.60217657 * 10^(-19);

%lattice constants Gadolinium in Angstroms (orthogonal unit cell)
areal = 3.636*sqrt(3); % x-direction
breal = 3.636; % y-direction
creal = 5.873;

% Here a mistake happened: in reality the lattice parameter reads creal = 5.783

% modified c such that the crystal becomes a perfect hcp-structure
cmod = breal*sqrt(8/3);

V0mod = (areal.*breal.*cmod);
V0real = (areal.*breal.*creal);

% New unit cell parameters
a = areal * (V0real/V0mod)^(1/3);
b = breal * (V0real/V0mod)^(1/3);
c = cmod * (V0real/V0mod)^(1/3);

V0 = (a.*b.*c);

% changes by +/-N * step of the lattice constants will be calculated
N = 15;
step = 0.001;

% unnecessary lines in LAMMPS log
lines = 19;

% Bulk modulus of Gadolinium in GPa
Blit = 38;

% atom configuration in one primitive cell and equilibrium volume V0
A = [0 0 0; b/sqrt(3) 0 c/2; a/2 b/2 0; b*5/(2*sqrt(3)) b/2 c/2];

% Initialize matrices for volume and atom positions

```

```

V = zeros(1,N+1);
P = zeros(size(A));

% Prepare the structure files for LAMMPS in the next loop
for j=-N:(N+1)
    anew = (a*(1+j*step));
    bnew = (b*(1+j*step));
    cnew = (c*(1+j*step));

    % open new structure file
    unix(sprintf('cp template_structure ./LAMMPS/structure_file%i',j));

    % add lattice parameters to structure_file
    FindAndReplace(sprintf('./LAMMPS/structure_file%i',j), ...
                    'aLattParam',sprintf('%f',anew));
    FindAndReplace(sprintf('./LAMMPS/structure_file%i',j), ...
                    'bLattParam',sprintf('%f',bnew));
    FindAndReplace(sprintf('./LAMMPS/structure_file%i',j), ...
                    'cLattParam',sprintf('%f',cnew));

    structure_file = fopen(sprintf('./LAMMPS/structure_file%i',j),'a');

    % calculate new atom positions and the primitive cell's volume
    P = (1+j*step).*A;
    V(j+N+1) = anew*bnew*cnew;

    % Prepare P for output
    P = [[1:4]' ones(4,1) P];

    % append atom positions to new structure_file
    fprintf(structure_file,'%i %i %f %f %f\n',P');

    fclose(structure_file);
end

% Starting point for fit
start = [100 10 10];

% initial guess for the equilibrium energy of one primitive cell in eV
epsilon = zeros(100,1);
epsilon(1) = 0.25;
epsilon_low = 0.09;
epsilon_high = epsilon(1);

% control used to end while loop once sufficient B0 has been calculated;
% number of dine loop iterations saved in count
control = 0;

```

```

count = 1;

% initialize some matrices:
% will be used to save the minimum total potential energy of a unit cell
% at V0 for every epsilon
minE = zeros(100,1);

% Used to store the Bulk moduli for each epsilon
BO = zeros(100,1);

% Stores all tried epsilon values
epsilonold = zeros(100,1);

% Total potential energies of the unit cell for each tried epsilon
E = zeros(100,2*N+1);

while control ~= 1
    for j=-N:(N+1)
        %Open and modify LJ_for_fit%i.dat (input for LAMMPS)
        unix(sprintf('cp template_LJ_for_fit.dat ...
            ./LAMMPS/LJ_for_fit%i.dat',j));
        unix(sprintf('sed -i ''8i read_data structure_file%i'' ...
            ./LAMMPS/LJ_for_fit%i.dat',j,j));

        % Add cutoff and sigma to LAMMPS input file; cutoff set to be 5 times sigma
        % (see: https://en.wikipedia.org/wiki/Lennard-Jones\_potential)
        sigma = 2^(-1/6)*b*1.029;
        cutoff = sigma.*5.5;

        % Prepare LAMMPS input
        FindAndReplace(sprintf('./LAMMPS/LJ_for_fit%i.dat',j),'cutoff1', ...
            sprintf('%f',cutoff));
        FindAndReplace(sprintf('./LAMMPS/LJ_for_fit%i.dat',j),'epsilon', ...
            sprintf('%f',epsilon(count)));
        FindAndReplace(sprintf('./LAMMPS/LJ_for_fit%i.dat',j),'sigma', ...
            sprintf('%f',sigma));

        % Run LAMMPS calculation of the total potential energy
        cd LAMMPS;
        unix(sprintf('./lmp_serial < LJ_for_fit%i.dat',j));
        log = fopen(sprintf('file.log'),'r');

        % remove unnecessary lines from file
        for i=1:lines
            fgetl(log);
        end
    end
end

```

```

    % Get total potential energy of a unit cell from LAMMPS output
    tmp = fscanf(log,'%f',6);
    E(count,j+N+1) = tmp(5);

    fclose(log);
    cd ..;
end

% fit according to BIRCH-MURNAGHAN equation of states
fit1 = birchmurnaghanfit(V',E(count,:)',VO,start);

plot(fit1,'k-',V,E(count,:),'kv')
grid on;

xlabel('Volume $V$ of the unit cell [\AA$^3$'],'interpreter','latex', ...
      'FontSize',16);
ylabel('Potential energy $E$ [eV]','Interpreter','latex','FontSize',16);

s1 = sprintf('Data from LJ potential with \n $\epsilon$ = %g eV and ...
            $\sigma$ = %g \AA',epsilon(count),sigma);
s2 = sprintf('Birch-Murnaghan fit with $V_0$ = %g \AA$^3$',VO);

legend1 = legend(s1,s2);
set(legend1,'Interpreter','latex','FontSize',12,'Location','North');

% fit coefficients
C = coeffvalues(fit1);
sigmaC = confint(fit1,0.95);

% Convert from ev/angstrom^3 to GPa
B0(count) = C(2)*1.602*10^2;

picture = sprintf('%i_%geV_%gGPa.eps',count,epsilon(count),B0(count));
print('-depsc2',picture);

if (abs(Blit-B0(count))/Blit)< 0.0001
    control = 1;
    break
else
    start = C;

    if B0(count) < Blit
        epsilonlow = epsilon(count);
        epsilonold(count) = epsilon(count);
        epsilon(count+1) = (epsilonup - epsilonlow)/2+epsilonold;
    else
        epsilonup = epsilon(count);

```

```

        epsilonold(count) = epsilon(count);
        epsilon(count+1) = (epsilonup - epsilonlow)/2+epsilonlow;
    end

    count = count + 1;
end

fprintf(fitPotentiallog, '%i %f %f\n', count, epsilon(count), B0);

end

figure(3);
fit2 = fit(epsilon(1:count), B0(1:count), 'poly1');
Cfit2 = coeffvalues(fit2);

plot(fit2, 'k-', epsilon(1:count), B0(1:count), 'kv');

ylabel('Bulk modulus $B_0$ [GPa]', 'interpreter', 'latex', 'FontSize', 20);
xlabel('LJpotential depth $\epsilon$ [eV]', 'interpreter', 'latex', 'FontSize', 20);
grid on;
s1 = sprintf('Data points from fitting procedure');
s2 = sprintf('Linear fit $a \cdot x + b$: \n$a=${1.3e m^{-3}}$, ...
            $b=${1.3f GPa}', (Cfit2(1)/e), Cfit2(2));

legend3 = legend(s1, s2);
set(legend3, 'Interpreter', 'latex', 'FontSize', 12, 'Location', 'NorthWest');

picture = sprintf('B0_vs_epsilon.eps', count, epsilon(count), B0(count));
print('-depsc2', picture);

```

The external fit function birchmurnaghanfit.m:

```

-----birchmurnaghanfit.m-----
% input vectors E and V must be column vectors and have to have the same
% length

function myfit1 = birchmurnaghanfit(V,E,V0,start)

    myfittype1 = fittype('A+9*Vzero*B/16*((Vzero/V)^(2/3)-1)^3 * C + ...
        + ((Vzero/V)^(2/3)-1)^2 * (6-4*(Vzero/V)^(2/3))', ...
        'independent', 'V', 'dependent', 'E', 'problem', 'Vzero', ...
        'coefficients', {'A', 'B', 'C'});

    myfit1 = fit(V,E,myfittype1, 'Maxiter', 10000, 'Robust', 'Bisquare', 'StartPoint', ...
        start, 'problem', V0)
end

```

The external function `FindAndReplace.m`:

```
-----FindAndReplace.m-----

function FindAndReplace(filename,oldword,newword)

    fr = sprintf('sed -i ''s/%s/%s/g'' %s',oldword,newword,filename)
    unix(fr);

end
```

The LAMMPS input template to calculate the total potential Energy of a unit cell:

```
-----template_LJ_for_fit.dat-----

log file.log

units metal
newton on
boundary p p p

atom_style atomic

pair_style lj/cut cutoff
pair_coeff * * epsilon sigma cutoff
run 0
```

`epsilon`, `sigma`, `cutoff` need to be replaced by the appropriate values (done in `fit_potential.m` by using the function `FindAndReplace.m`). The structure file template which specifies the number of atoms per unit cell, their mass and the unit cell dimensions:

```
-----template_structure-----

Crystalline Gd (in Angstroms)

4 atoms # number of atoms
1 atom types # number of atom types

# unit cell parameters a, b and c
0.00000 aLattParam xlo xhi
0.00000 bLattParam ylo yhi
0.00000 cLattParam zlo zhi

Masses

1 157.14 # atom type / atomic weight

Atoms # atom list
```

## A.2. Thermal vibrations simulation

The input file used to calculate 100 snapshots of the vibrating crystal structure:

```
log file.log

units metal

timestep 0.01
newton on
boundary p p p

atom_style atomic
read_data structure_file_prep

pair_style lj/cut 18.2751
pair_coeff * * 0.1157 3.3228 18.2751

# print thermodynamic data every N timesteps
thermo 100

# Get initial atom positions
dump atomdata all atom file_1_initial.MD
run 0

# Simulate the equilibrating processes & shoot movie
dump atomdata all atom file_1_initial.MD
dump mov1 all movie 10 movie.avi type type size 600 720

velocity all create <TEMPERATURE> 299792458
fix fix1 all nvt temp <TEMPERATURE> <TEMPERATURE> 0.01 <DRAG>

run 5000

# Calculate 99 snapshots of the vibrating crystal structure
dump atomdata all atom file_1.MD

fix fix1 all nvt temp <TEMPERATURE> <TEMPERATURE> 0.01 <DRAG>
run 495000
```

<TEMPERATURE> needs to be set to the temperature one wants to simulate and <DRAG> may be set to damp temperature fluctuations effectively. The structure input file `structure_file_prep` contains the undisturbed, perfect crystal structure of the simulation super cell. Compare section